Carnegie Observatories Astrophysics Series, Vol. 3:
Clusters of Galaxies: Probes of Cosmological Structure and Galaxy Evolution, 2004
ed. J. S. Mulchaey, A. Dressler, and A. Oemler (Cambridge: Cambridge Univ. Press)

Probing Dark Matter in Clusters

IAN SMAIL
Institute for Computational Cosmology, University of Durham, UK

Abstract

Gravitational lensing provides a unique probe of the distribution of mass in clusters on scales from 10 kpc out to the turn-around radius at ~ 5 Mpc. I review how lensing has been used to investigate the total mass in the central regions of clusters, before discussing more recent work tracing the form of the mass distribution in cluster cores, and finally touching on how lensing is being used to map the environment of galaxies and determine how this affects their dark matter halos and star formation histories.

1.1 Introduction

To produce an Einstein ring image of a suitably positioned distant source, a foreground gravitational lens has to focus multiple light paths onto the observer. To achieve this, the mass density in front of the source must exceed a critical mass surface density of around $0.5\,\mathrm{g\,cm^{-2}}$ (or $2.4 \times 10^9 M_\odot\,\mathrm{kpc^{-2}}$). The projected mass in the central regions of the most massive, intermediate-redshift clusters is of the order of $\sim 10^{14} M_\odot$ within a radius of 50–100 kpc, and these regions therefore exceed the density threshold required for producing multiple images of cosmological sources.

The study of gravitational lensing by clusters is a relatively young field; the first papers presenting observational evidence for gravitational lensing by clusters were published in the late 1980s (Soucail et al. 1988; Hammer et al. 1989; Lynds & Petrosian 1989; Wambsganss et al. 1989). The field developed rapidly in the 1990s (e.g., Kochanek 1990; Tyson, Wenk, & Valdes 1990; Blandford & Narayan 1992), producing a near-exponential growth in the number of refereed publications (Fig. 1.1), which now approaches $\sim$100 papers per year.

The growth of research on cluster lenses reflects their usefulness as a tool to tackle a wide variety of questions in observational cosmology, including constructing mass-selected samples of distant clusters, surveys of the faintest galaxies, active galactic nuclei, or supernovae in the distant Universe, constraining the properties of dark matter, confirming the presence of mass over-densities associated with high-z structures, searches for dark halos, and tests of cosmological parameters. This review discusses how lensing can be used to address three problems that are relevant for this Symposium:

- Comparing X-ray and lensing masses for clusters
- Measuring the mass profile of clusters
- Relating galaxy properties to their local mass density

For simplicity, the content of this written review has a stronger focus on published results

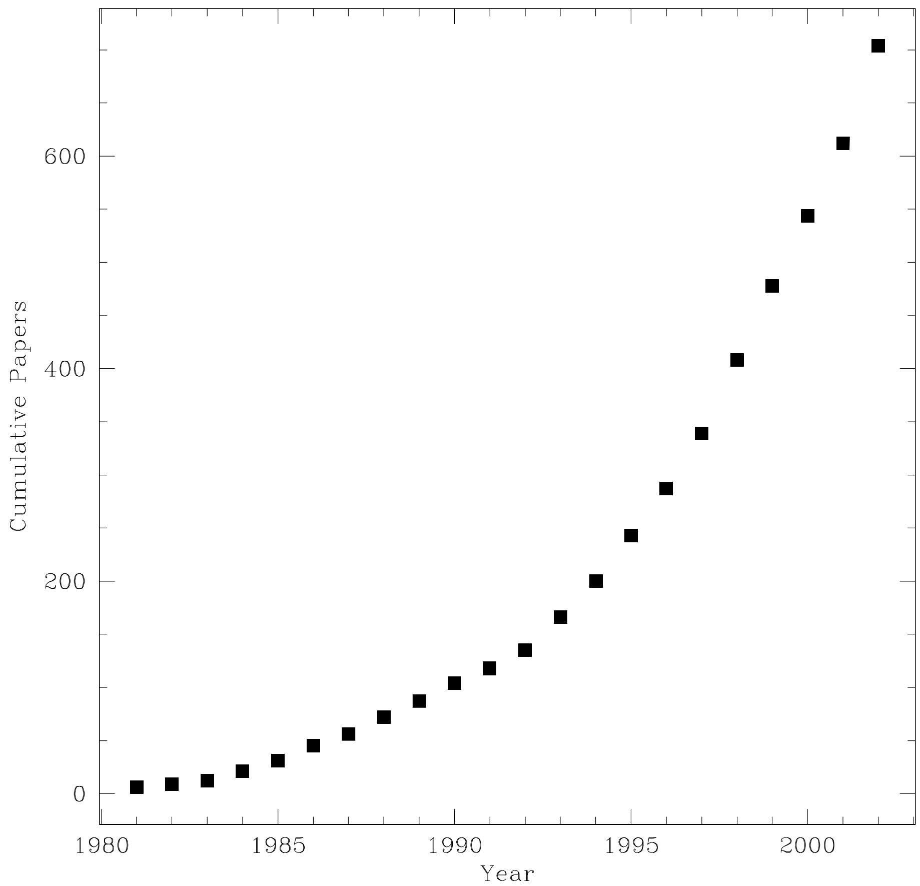

Fig. 1.1. Cumulative refereed publications dealing with gravitational lensing by clusters as listed on ADS (January 2003). The accelerated growth after 1993 reflects the refurbishment of *HST* and the development of new techniques for extracting the 2-dimensional mass distributions from weak shear observations.

than did the oral presentation at the Symposium. For consistency with the usage in the reviewed work, we assume $H_0 = 50\,\mathrm{km\,s^{-1}\,Mpc^{-1}}$ and $q_0 = 0.5$ throughout.

1.2 Lensing Methods

The first goal of any cluster lensing study is to derive an accurate understanding of the amount and distribution of mass within the cluster. For some applications this is also the only goal; however, it is frequently just a step on the way to exploiting the cluster lens for other purposes. Techniques to determine the mass distribution within a cluster lens can be crudely divided into two different approaches: parametric and non-parametric methods.

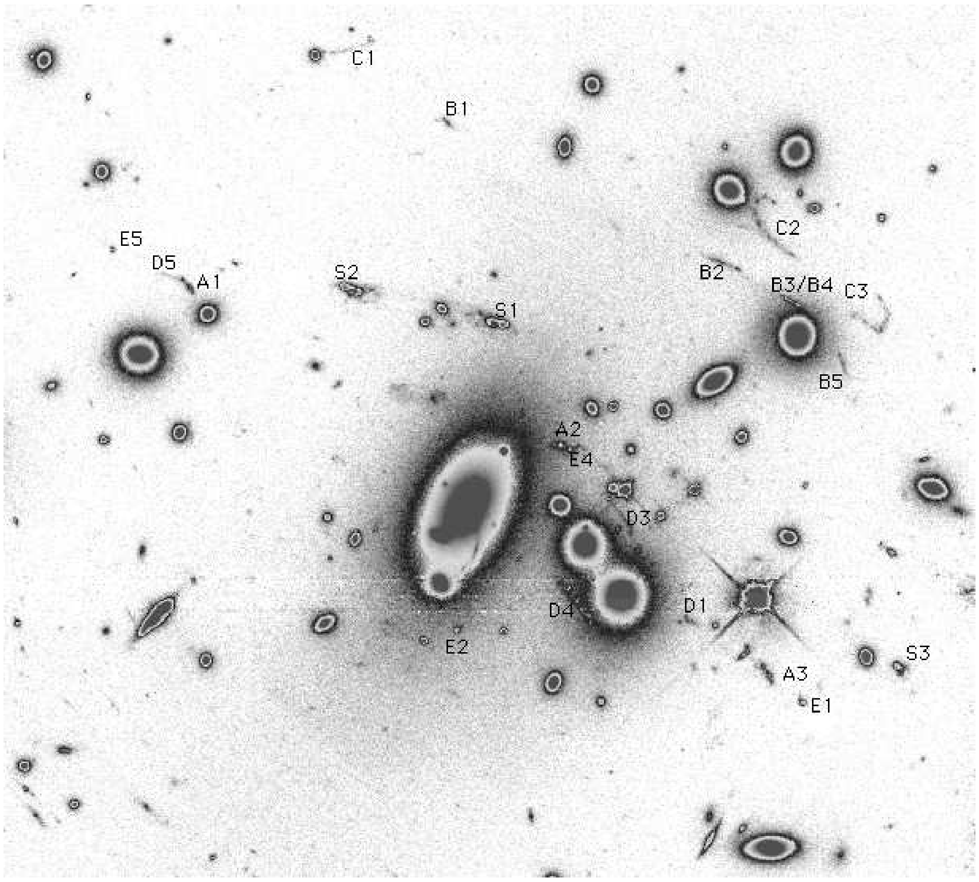

Fig. 1.2. The core region of the $z = 0.31$ cluster AC 114 as seen in a deep *HST* WFPC2 F702W image. This graphically demonstrates the power of *HST* for morphologically identifying the multiple images of background galaxies, such as C1-C2-C3 at $z = 2.86$ or the $z = 1.87$ galaxy S1-S2-S3 (Smail et al. 1995; Campusano et al. 2001). I mark the various images of the six multiply imaged background galaxies (S, A–E), which are visible through the cluster core. The field shown is $50'' \times 50''$ in extent, and the lensed features precisely constrain the distribution of mass within the cluster core on scales from $\sim 20 - 150$ kpc (Natarajan et al. 1998).

1.2.1 Parametric Lens Modeling

One cause of the rapid rise of publications dealing with lensing by clusters was the refurbishment of the *Hubble Space Telescope* (*HST*) and the installation of the Wide Field and Planetary Camera 2 (WFPC2) in 1993. This has produced a uniquely powerful instrument for lensing studies, combining excellent image quality, depth, and image stability. The fine spatial resolution of *HST* means we can compare the morphologies of candidate multiply imaged galaxies (Fig. 1.2) to confirm their identifications (e.g., Smail et al. 1995; Tyson et al. 1998; Bézecourt et al. 1999). In addition, it facilitates the identification of faint, lensed features against the crowded background of diffuse halos of the elliptical galaxies in the cores of massive clusters. The sensitivity, resolution, and stability of *HST* are also well suited to searching for the weaker signals of gravitational lensing on much larger scales around clusters, by detecting and reliably measuring the shapes of large numbers of weakly distorted arclets.

The first parametric studies of the mass distribution within clusters, however, predated *HST* and had to rely on deep ground-based imaging (Hammer et al. 1989). These studies reconstructed the dark matter distribution within clusters using simple parametric representations of the mass, guided by the distribution and extent of the light in these systems (e.g., Kneib et al. 1993). With higher-quality observations from *HST*, such studies have now become much more refined, yielding constraints from both strong and weak lensing regimes and allowing for a large number of mass components within the clusters (Kneib et al. 1996; Abdelsalam, Saha, & Williams 1998; Tyson et al. 1998).

These models rely on the identification of multiply imaged background sources, where we can see N images of the same galaxy. Each multiply imaged source provides $3N$ observables: position + flux of each of the images. There are 3 unknowns for the source (its position on the source plane and flux), and hence $3(N-1)$ constraints are available to model the lens. The best-studied strong lenses, those with deep *HST* imaging, can have several multiply imaged background sources. For example, Figure 1.2 shows the central region of the cluster lens AC 114. This area contains 21 images of six different background galaxies, three quintets and three triplets, at redshifts between $z = 1.50$ and $z = 3.35$ (Campusano et al. 2001).

Using these multiply imaged sources, as well as the weak shear field on somewhat larger scales, a model can then be constructed using a series of large-scale potentials to represent the cluster (and any large sub-clumps) and galaxy-scale mass components tied to individual cluster members. The positions, masses, orientations, ellipticities, and radial profiles of these components can all be fit, although to restrict the number of free parameters the masses of the galaxies are usually required to follow a simple scaling relation based upon their luminosities, and their other parameters are similarly fixed to those of their light distributions (Natarajan et al. 1998). Such models have now been constructed for over a dozen clusters (Kneib et al. 1996; Smith et al. 2001, 2004; Figs. 1.3 and 1.4), and the bulk of this review deals with results derived from this "strong" lensing technique.

1.2.2 Non-parametric Techniques

The development of non-parametric techniques to recover the mass distribution in clusters from observations of the weakly sheared arclets provided a second major impetus to work on gravitational lensing by clusters (Kaiser & Squires 1993; see also Tyson et al. 1990). These techniques use the coherence of the weak distortion imprinted on the shapes of faint, randomly oriented background galaxies to recover the lensing signal and hence trace the mass distribution out to the turn-around radius, ~ 5 Mpc or $\sim 0.25°$ for a massive cluster at $z \approx 0.2$. These techniques have been applied to clusters from $z \approx 0.1$ to $z \approx 1$ and provide our only "true" images of the distribution of mass in clusters. They are also well adapted to searches for distant clusters by identifying the lensing signature they produce in the shapes of faint field galaxies, as demonstrated by several speakers at this Symposium (see Margoniner 2004 and Margoniner et al. 2004).

Recent refinements have included more complex approaches to measuring galaxy shapes and correcting for the aberrations induced by the telescope optics (Kaiser, Squires, & Broadhurst 1995; Refregier & Bacon 2003), the incorporation of weak and strong lensing constraints within the reconstruction, and improvements to the stability of the techniques in

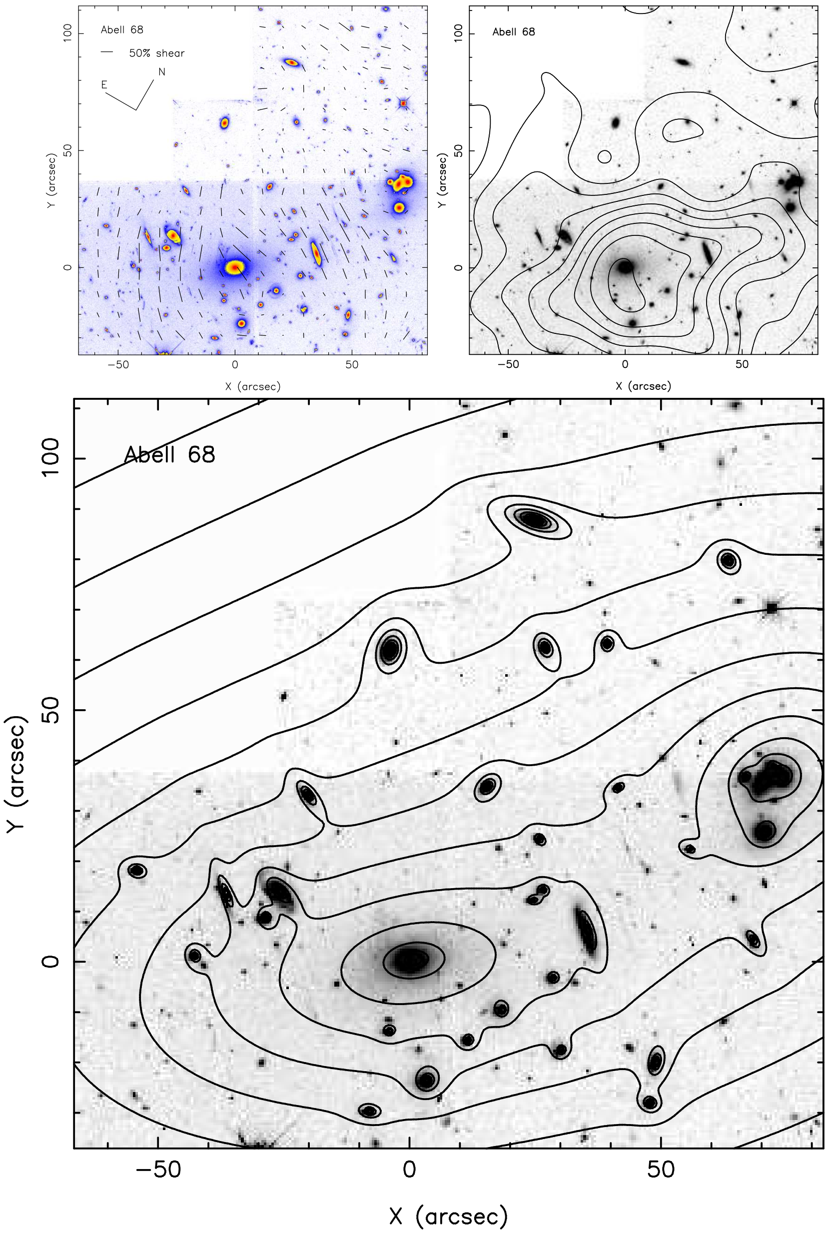

Fig. 1.3. Three representations of the $z = 0.21$ cluster Abell 68, one of the X-ray luminous clusters included in the *HST* lensing survey of Smith et al. (2004). These panels each show the F702W exposure of the cluster core. In the top-left panel, the *HST* image is overlaid with a vector field representing the lensing-induced shear signal. This is constructed by simply averaging the shapes of faint galaxies seen through the cluster core. The shear field identifies a saddle region in the potential between two main mass concentrations. This bimodality is less obvious, but still visible, in the X-ray image of this cluster, which is shown as the contour map in the top-right panel. The bottom panel illustrates, as a logarithmically spaced contour plot, the best-fitting mass model constructed for the cluster by Smith et al. (2004). The secondary clump to the north-west of the central cD contains roughly 30% of the total mass of the core.

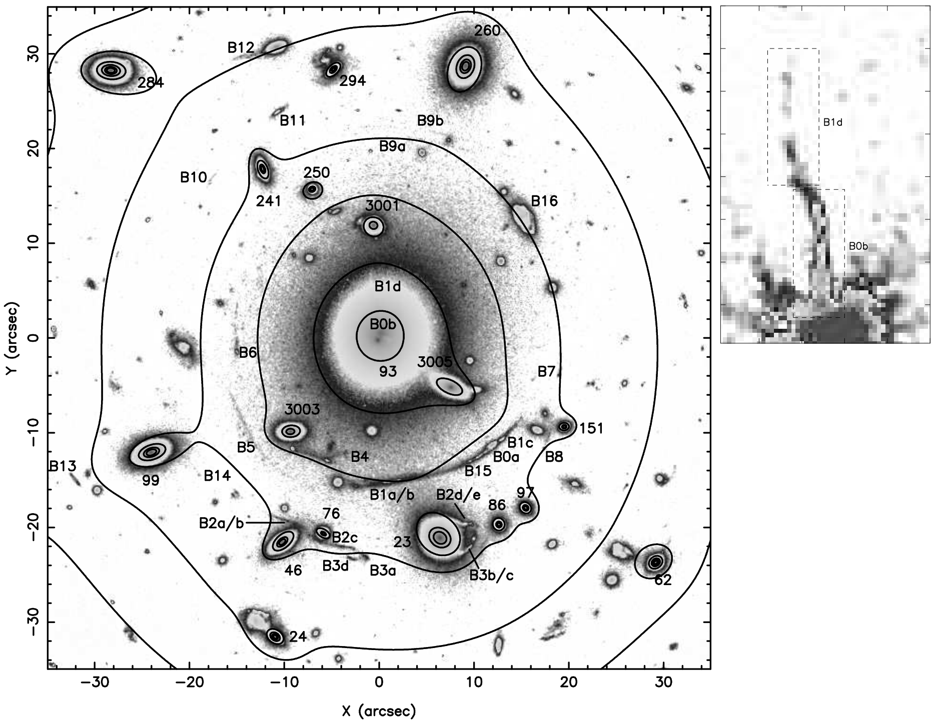

Fig. 1.4. An *HST* WFPC2 F702W image of a $70'' \times 70''$ region in the core of Abell 383, overlaid with isodensity contours illustrating the lens model of Smith et al. (2001). The alphanumeric labels identify multiply imaged background galaxies and arclets used in the lens modeling, while the numerical labels show the galaxy-scale masses incorporated in the model. The central galaxy shows what appears to be a dust lane across its center, as well as two radial features, B0b and B1d, which are highlighted in the panel to the right. These features are interpreted as radial arcs associated with the same $z \approx 1.0$ background galaxies that produce the main giant arcs (B0 and B1). These radial arcs provide strong constraints on the form of the mass profile in the very center of the cluster. The mass contours in the main panel correspond to projected surface densities of $(0.3, 0.4, 0.6, 0.8, 1.1, 1.5) \times 10^{10} M_{\odot}$ kpc^{-2}. See Smith et al. (2001), from which this figure is adapted, for more details.

the presence of noise (e.g., Seitz, Schneider, & Bartelmann 1998; Marshall et al. 2002). Non-parametric mass reconstructions are also possible based upon the magnification of the background field population, although to date these have not been so widely developed (Dye et al. 2002).

1.2.3 Cosmic Magnifying Glasses

The magnification produced by cluster lenses can be used as an aid in studying any population of extragalactic sources that is faint, distant, and relatively numerous. Indeed, lensing-boosting is now becoming a standard technique in studies of very faint populations in the distant Universe. For example, the quality of the rest-frame UV spectroscopy of the galaxy cB58 at $z = 2.72$ rivals that of the best-studied galaxies in the local Universe, as a result of its substantial magnification by a foreground cluster lens (Pettini et al. 2002).

Similarly, narrow-band searches for emission-line galaxies at the highest redshifts have also benefited from the added boost of a foreground lens (Hu et al. 2002), while studies of intrinsically faint sources selected in the near-infrared or submillimeter wavebands have provided unique insights into the properties of these populations (Cowie, Barger, & Kneib 2002; Smail et al. 2002; Smith et al. 2002; Wehner, Barger, & Kneib 2002).

Abell 2218 provides a good example of how versatile a single well-constrained lens can be. This rich cluster lies at $z = 0.18$, and its core contains at least nine recognizable multiply imaged background sources, which produce in total 29 images. As a result the mass model for this cluster has been very well constrained, allowing it to be used for detailed studies of the properties of very faint and very distant galaxies. The nine multiply imaged sources lie in a region of the sky directly behind the cluster core, which is roughly $10'' \times 10''$ in size. This area contains an I = 23.5 mag $z = 2.52$ star-forming galaxy (Ebbels et al. 1996), an I = 26 mag submm-bright "extremely red object" also at $z \approx 2.6$ (van der Werf et al. 2004), and finally an I = 30 mag proto-galactic clump at $z = 5.6$ (Ellis et al. 2001), all of which are magnified by factors of 10–30. Just outside this area lies an I = 21.5 mag spiral galaxy at $z = 1.03$ with a resolved rotation curve (Swinbank et al. 2004). The discovery and detailed study of these galaxies have benefited substantially from their position behind the core of one of the most massive and best-constrained cluster lenses on the sky. Such regions provide an unique opportunity to study ultra-faint galaxies in a level of detail that will be otherwise unavailable until the advent of 30-m telescopes.

1.3 Comparing X-ray and Lensing Masses

Gravitational lensing provides a completely independent method to estimate the mass of clusters, free of many of the uncertainties associated with using indirect tracers. For example, when using the dynamics of cluster members, orbital characteristics and the virial state of the sample have to be assumed. Or, when modeling the X-ray emission from the intracluster medium, hydrostatic conditions have to be adopted and also a high degree of symmetry in the system has to be assumed to reliably deproject the mass distribution (Brainerd et al. 1998). Lensing, of course, has its own drawbacks: the shear signal is weak, and corrections need to be applied to remove instrumental effects. The strength of the lensing signal also depends not only on the mass of the cluster, but also on the redshifts of the background population that are used in the analysis. These are typically very faint galaxies for which redshifts have to be statistically estimated based on photometric redshift surveys of regions such as the Hubble Deep Field. Nevertheless, lensing provides an important, independent technique to derive cluster masses, and so there is considerable interest in comparing the various mass estimators, in particular lensing and X-ray estimates, to see how well they agree.

A number of early comparisons of the X-ray and lensing mass estimates of clusters on < 1 Mpc scales, mostly from strong lensing constraints, found significant differences, with the lensing-derived masses typically being a factor of 2–3 larger than the X-ray masses (Miralda-Escudé & Babul 1995; Wu & Fang 1997). Explanations for this offset included the projection onto the cluster cores of unrelated structures that artificially increase the lensing-derived masses, or proposed mechanisms to provide nonthermal pressure support to reduce the X-ray estimates.

- AGREE, $M_{\rm lens}/M_{\rm X} \approx 1$: MS 1008–12, $z = 0.31$; RX J1347–11, $z = 0.45$; MS 0016+16, $z = 0.55$ (Fischer & Tyson 1997; Schindler et al. 1997; Sahu et al. 1998; Allen, Schmidt, & Fabian 2002; Ettori & Lombardi 2003; Worrall & Birkinshaw 2003).
- DISAGREE, $M_{\rm lens}/M_{\rm X} \approx 2-3$: Abell 1689, $z = 0.18$; MS 0440–02, $z = 0.19$; MS 1008–12, $z = 0.31$; Cl 0500–24, $z = 0.32$; Abell 370, $z = 0.37$; Cl 0024+16, $z = 0.39$ (Gioia et al. 1998; Ota, Mitsuda, & Fukazawa 1998; Soucail et al. 2000; Athreya et al. 2002; Xue & Wu 2002; Ota et al. 2004).

The lists above give a random selection of X-ray/lensing mass comparisons from the recent literature. This shows that the situation is still confused, with groups claiming either agreement or disagreement between the two estimates, sometimes for the same clusters. Many of these studies can be criticized for adopting overly simplistic models for their lensing or X-ray analyses, or for concentrating on the same small set of well-known cluster lenses. However, the criticisms are not unique to one or other set of studies; rather, the situation seems to reflect a real diversity in the cluster properties.

What is the origin of disagreements in the mass determinations for some clusters? Does it reflect an oversimplification or misapplication of assumptions in one or other of the mass estimates, or a real physical effect? Allen (1998) answered these questions by reassessing the X-ray data for a mixed sample of 13 clusters (all known strong lenses) containing both examples where the lensing and X-ray masses agreed, and those where they disagreed.

Allen used *ROSAT* HRI X-ray images and *ASCA* temperatures for the clusters. To determine the mass profile of these clusters, he applied a standard X-ray deprojection analysis, which required an isothermal X-ray temperature profile, and accounted for the contribution from any cold gas in the cluster core to the measured X-ray temperatures. Combining these mass estimates with those from simple lens models for the clusters, he found a wide range in $M_{\rm lens}/M_{\rm X}$ (Fig. 1.5). However, the clusters with centrally peaked X-ray emission, which have high central gas densities and short inferred cooling times for the gas (I will use the possible misnomer "cooling flow" to identify this class), do have $M_{\rm lens}/M_{\rm X} \approx 1$, while those clusters with lower central gas densities give discrepant values, $M_{\rm lens}/M_{\rm X} \approx 2-4$ (Fig. 1.5). Short gas cooling times have previously been interpreted as an indication of a relaxed system, suggesting that the non-cooling flow clusters may be dynamically more active. The cooling flow and non-cooling flow clusters are also distinguished by the size of the core radii in the cluster potentials, which are inferred from the deprojection analysis (Allen 1998). Cooling flow clusters typically have inferred core sizes of ~ 50 kpc, where as non-cooling flow clusters have best-fitting cores of > 250 kpc. These apparently large cores could be spurious and instead reflect the breakdown of hydrostatic equilibrium in the centers of these clusters, probably due to dynamical activity associated with mergers. Indeed, deprojecting the non-cooling flow clusters with a fixed ~ 50 kpc core radius produces mass estimates in much better agreement with those from lensing, $M_{\rm lens}/M_{\rm X} \approx 1.2 \pm 0.3$.

A comparison of the X-ray and lensing mass estimates (from both strong and weak lensing measurements) as a function of scale on which the masses are estimated is shown in Figure 1.5; to assure the reliability of both estimates, only cooling flow clusters are included at small scales. This shows good agreement between the two estimates over a very wide range in scale.

Thus, the origin of the disagreements between lensing and X-ray mass estimates appears to be the inappropriate application of X-ray analysis techniques, which assume hydrostatic

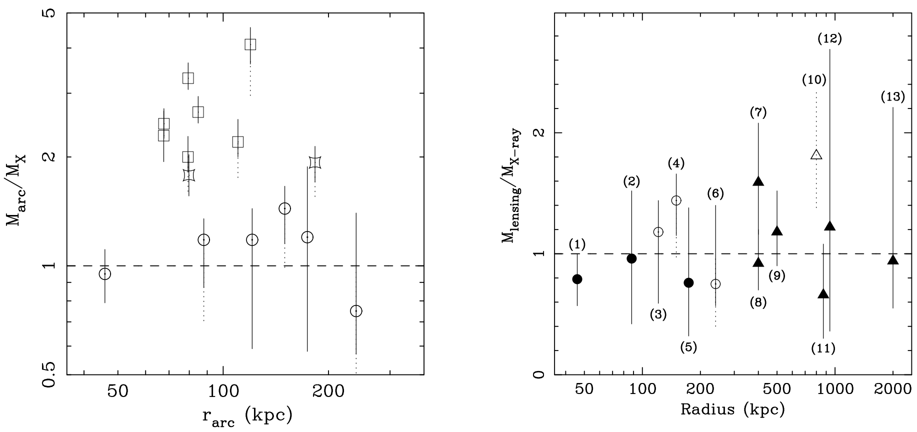

Fig. 1.5. The *left* panel shows the distribution on the $M_{\rm lens}/M_{\rm X} - r_{\rm arc}$ plane for those clusters with strongly peaked central X-ray emission ("cooling flow"; circles) and those with less-peaked X-ray emission (squares). The former systems show good agreement between the two mass estimates, whereas those with less centrally concentrated X-ray emission typically show low X-ray-estimated masses compared to their lensing values. The *right* panel shows a compilation of $M_{\rm lens}/M_{\rm X}$ estimates from the literature as a function of the scale of the measurements (see Allen 1998 for the meaning of the symbols and the references to the original work). At small radii, only clusters that exhibit strongly peaked X-ray emission are included in the figure. This figure demonstrates reasonable agreement between X-ray and lensing mass estimates over nearly 3 orders of magnitude in scale. Both figures are taken from Allen (1998).

equilibrium, to the core regions of clusters that may be far from equilibrium (most probably due to mergers). This problem is exacerbated by comparing the two estimates on small scales, where the X-ray analysis is particularly sensitive to these model assumptions.

Allen's (1998) conclusions prompt two important questions: (1) How frequently do the X-ray and lensing mass estimates for cluster cores disagree?" and (2) Can these discrepancies be directly related to merging in the clusters? To answer these requires a joint lensing and X-ray analysis of an unbiased sample of clusters. Smith et al. (2004) have undertaken such a survey using *HST* imaging and *Chandra* X-ray observations of 10 X-ray luminous clusters ($L_{\rm X} \geq 8 \times 10^{44}$ erg s^{-1}) in a narrow redshift range around $z = 0.2$, selected from the XBACS sample (Ebeling et al. 1996). The *HST* imaging provides the basis for detailed lensing models of the clusters, which can be compared to the results from the spectral analysis of the *Chandra* X-ray data on ~ 1 Mpc scales. The lensing and X-ray results for one of the clusters from the sample are shown in Figure 1.3, illustrating the level of detail available for the comparisons of the different baryonic and non-baryonic components within the clusters.

The Smith et al. (2004) survey answers both of the questions raised above. They find mass substructures (consisting of $\geq 10\%$ of the cluster mass) in half of the clusters in their sample (see also Dahle et al. 2002). The lensing and X-ray mass estimates are in good agreement for the regular clusters, but those clusters that exhibit substructure have X-ray temperatures measured across the central 1 Mpc that are $\sim$30% hotter at a fixed mass than the more regular clusters. The effectiveness of even relatively minor mass mergers in heating the intracluster gas and the prevalence of these minor mergers in the most X-ray luminous clusters clearly raises concerns over attempts to use X-ray observations to infer the detailed mass distribution in any clusters that show even hints of structural complexity. This is particularly true of clusters at higher redshifts, where the effects of infall are likely to have been more extreme. To test this expectation, a similar joint *HST*/*Chandra* analysis is being performed by the same group on an identically selected sample of X-ray luminous clusters at $z = 0.4$.

1.4 Cluster Mass Profiles

The next step beyond measuring the amount of mass in clusters with lensing is to derive their radial profiles. This endeavor has been given fresh impetus by the claims of a "universal mass profile" derived from *N*-body simulations of halos in a cold dark matter (CDM) cosmogony (Navarro, Frenk, & White 1997, hereafter NFW). On large scales the NFW profile falls off as $\rho \propto r^{-3}$, steeper than isothermal ($\rho \propto r^{-2}$), while on small scales the NFW profile flattens to $\rho \propto r^{-1}$, although it retains a central cusp. The exact details of the form of the mass profile are the subject of debate within the theoretical community (e.g., Ghigna et al. 2000), but the central claim that CDM halos have a relatively well-determined profile has not been contradicted and provides an observationally testable prediction for which lensing is particularly well suited.

One class of gravitationally lensed features are particularly useful for studying the mass distribution in the central regions of lensing clusters. These are the radial arcs found in the very centers of a handful of cluster lenses, mostly from *HST* imaging: MS 2137.3–23 (Fort et al. 1992; Mellier, Fort, & Kneib 1993), Abell 370 (Smail et al. 1996), AC 114 (Natarajan et al. 1998). While the giant, tangential arcs (e.g., B0/B1 in Fig. 1.4) provide a precise estimate of the total enclosed mass in the cluster centers, the positions of the radial arcs are sensitive to the local gradient of the mass profile, allowing us to model the mass on scales of < 100 kpc (Williams, Navarro, & Bartelmann 1999).

The mass profile derived from the lensing model of Abell 383 (Fig. 1.4) by Smith et al. (2001) on scales ≥ 10 kpc is dominated by the cluster-scale potential, the core radius of the cluster-scale mass distribution (~ 46 kpc) being consistent with previous estimates of core radii from lensing studies. The shape of Abell 383's mass profile is most precisely measured within $r \approx 100$ kpc, where constraints from the multiple images are available, and Smith et al. (2001) estimate the total projected mass within the radius of the giant arc (65 kpc) to be $(3.5 \pm 0.1) \times 10^{13} M_{\odot}$. The density profile of Abell 383 at the positions of the radial arcs (~ 20 kpc) is $d(\log\rho)/d(\log r) = -1.29 \pm 0.03$, intermediate between the NFW and Ghigna et al. (2000) predictions. However, the observed gradient includes a contribution from the baryonic component associated with the central galaxy of the cluster (Fig. 1.4), which is not included in the predictions of the dark-matter-only simulations. The unknown contribution of the central galaxy makes it nontrivial to compare the observations and predictions (see also Gavazzi et al. 2003).

To circumvent this problem, Sand, Treu, & Ellis (2002) and Sand et al. (2004) have been gathering velocity dispersion information for the central galaxies in clusters with radial arcs. This allows them to model and remove the contribution from the stars in the central galaxy, leading to much flatter mass profiles for the underlying dark matter, $d(\log\rho)/d(\log r) < -0.9$, in apparent conflict with the theoretical predictions for the dark matter profiles. Again, however, the comparison with theory is nontrivial, as it is not clear how the dark matter

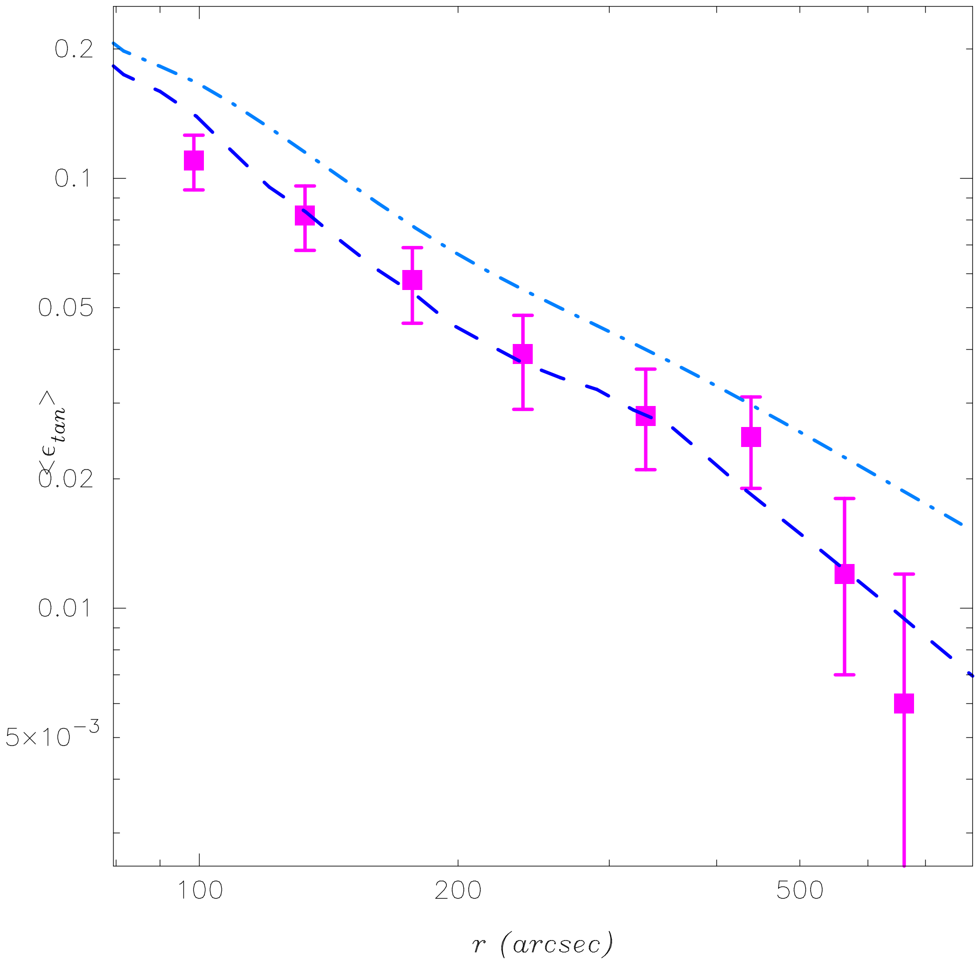

Fig. 1.6. The tangential shear profile ($\langle\epsilon_{\rm tan}\rangle$) around Cl 0024+16 from an analysis of the *HST* WFPC2 and STIS imaging of the cluster (Kneib et al. 2004). Isothermal (dot-dashed) and NFW (dashed) profiles are plotted; both are normalized to the strong-lens model of the cluster core. It is clear that the isothermal model grossly overpredicts the strength of the shear field out to the limit of the data.

distribution in the cluster core would react to the growth of the baryonic component of the central galaxy, if this was included in the theoretical simulations. Nevertheless, the necessary observations now exist, and the hope is that the modelers will rise to the challenge and produce more sophisticated "predictions" of the mass profile in cluster cores.

On larger scales, where the contribution from dissipational baryons should be less of a concern, the mass profile of clusters is being studied using weak shear techniques, primarily through comparisons of the observed and predicted shear profiles. Ground-based, panoramic imaging of three intermediate-redshift clusters is discussed by Clowe & Schneider (2001, 2002), who conclude that their data are insufficient to strongly differentiate between a singular isothermal sphere and a NFW profile on scales of 0.13–2 Mpc. To improve on this situation, Kneib et al. (2004) obtained a sparse mosaic of *HST* WFPC2 and STIS pointings covering a 5 Mpc region around the $z = 0.39$ cluster Cl 0024+16. Using the higher-fidelity imaging available from space, they were able to trace the mass profile from the core out to ~ 4 Mpc and strongly reject an isothermal mass distribution, finding instead that the NFW model provides an acceptable description of the mass profile on Mpc scales in at least this cluster (Fig. 1.6). Clearly, it is important to extend this approach to a larger sample of clusters to observationally determine the true *universality* of the mass profile.

1.5 Relating Galaxy Properties to their Dark Matter Environment

The final section of this review focuses on the application of gravitational lensing to obtain an even more detailed view of the mass distribution within clusters: on the scales of galaxy halos.

The weak shear induced in the shapes of background field galaxies by a foreground cluster lens reflects not only the large-scale distribution of mass within the cluster, but also the mass associated with individual cluster members. The latter can be studied by *stacking* the weak shear signal around each galaxy, where the contribution from the cluster-scale potential acts as an incoherent source of noise in the galaxy's reference frame, allowing the lensing contribution of the halos of the ensemble of galaxies to be recovered.

Natarajan et al. (1998) constructed a detailed lens model for the cluster AC 114 based on a wide-field *HST* mosaic. Their model incorporated small-scale perturbations associated with the halos of individual galaxies, and they then employed this model to constrain the properties of different populations of cluster galaxies. By adopting simple scaling relations between the radial extent and central velocity dispersion of the galaxies, both scaling with their optical luminosities, it is possible to constrain these parameters for a fiducial L^* cluster galaxy (Brainerd, Blandford, & Smail 1996).

They were able to show that the dark matter halo of a typical L^* spheroidal cluster galaxy is roughly 15 kpc in extent, much smaller than the ≥ 150 kpc inferred for similar luminosity galaxies in the field (Brainerd et al. 1996). This strongly suggested that the high-density cluster environment is truncating the dark matter halos of the galaxies. Unfortunately, the sample of early-type galaxies was too small to convincingly detect differences in the halo properties of elliptical and lenticular galaxies, although there was a hint that the halos of S0s could be less extended than those of ellipticals at a fixed luminosity.

Natarajan et al. (2002) extended this analysis to a larger sample of intermediate-redshift clusters for which *HST* imaging was available and which exhibit strongly lensed features suitable for constructing a detailed mass model. The best-fitting galaxy parameters from these mass models confirmed that typical L^* cluster galaxies are more compact than their field counterparts. However, when the truncation radii of the galaxies are plotted against the central density of their host clusters, a more intriguing correlation is found (Fig. 1.7). We see that the clusters with higher central densities have galaxy populations with smaller dark matter halos. The slope of this correlation agrees with that expected from tidal stripping of the halos by the cluster potential. This is arguably one of the few direct pieces of evidence for the interaction of galaxies with their environment. If correct, it underlines the importance of halo stripping on the dynamical evolution of galaxies lying within the infall regions of clusters. Relating the stripping of dark matter halos to the star formation history of the galaxies residing within them will provide important insights into how galaxies react to

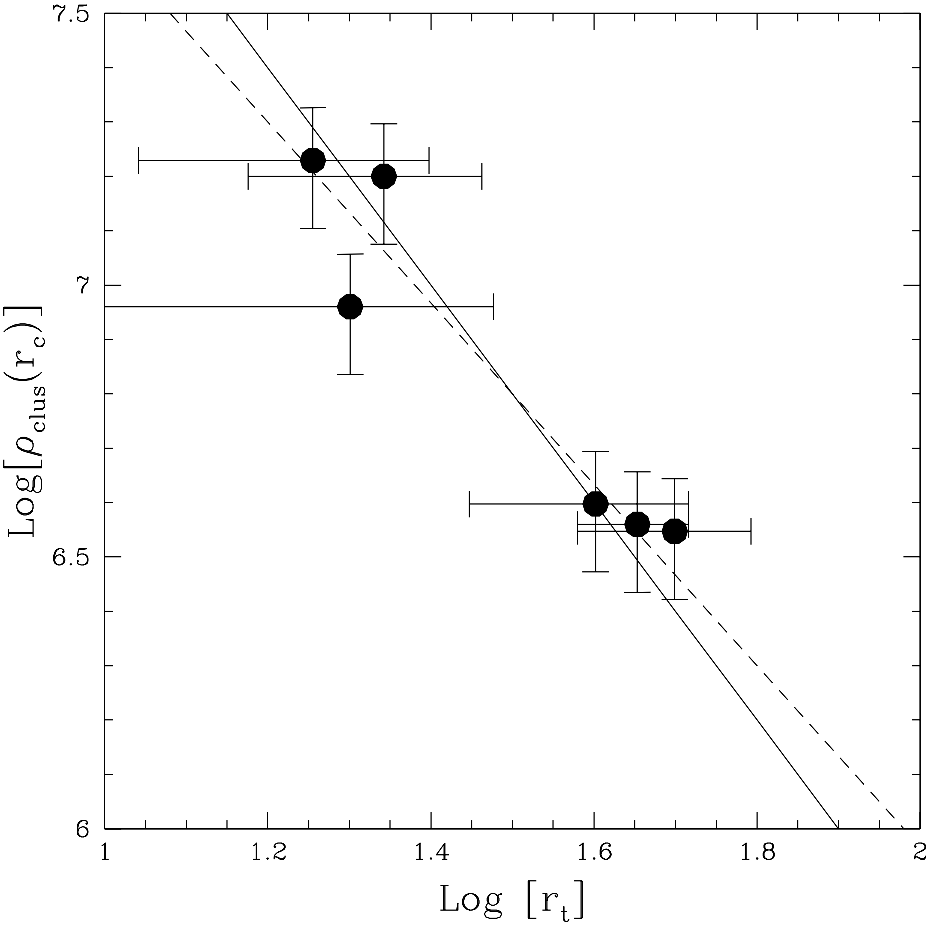

Fig. 1.7. The tidal radii of galaxies as a function of the central mass density in the clusters in which they reside. The dashed line shows the least-squares fit to the data, which gives a best-fit power-law index ($r_t^* \propto \rho^\beta$) of $\beta = -0.6 \pm 0.2$, in good agreement with the theoretical prediction of $\beta = -0.5$ from a tidal-stripping model (Natarajan, Kneib, & Smail 2002).

changes in their halos and also how they interact with the wider dark matter environment (Gray et al. 2002, 2004).

1.6 Summary

Gravitational lensing provides an increasingly important tool for investigating the distribution of mass in clusters. The information from lensing studies can be compared and contrasted to other tracers of cluster mass to address a range of questions about the formation and evolution of clusters and their component galaxies.

Comparison of X-ray and lensing mass estimates within the virial radii of rich clusters shows reasonable agreement for systems where both approaches can be reliably employed.

However, there is evidence that X-ray measurements of the masses of merging systems are systematically in error, even for relatively minor mergers (1:10 mass ratios).

On large scales the projected mass profile of clusters appears to roughly follow the form predicted from hierarchical models using a CDM power spectrum. The form of the mass profile in the cores of the halos is also similar to the theoretical predictions, but this may be a coincidence as the observations indicate substantially flatter dark matter profiles than theory predicts when the dominant baryonic component (associated with the central galaxy) is removed. However, predictions are based on dark-matter-only simulations, and hence the behavior of the combined baryonic and dark matter profile has not yet been accurately modeled.

Finally, the behavior of the massive halos associated with individual galaxies within clusters suggests that these are affected by their environment. There are indications that this behavior follows that expected from tidal stripping in the cluster potential well. Future work on this issue, focusing on the effects on the star formation history of the galaxies residing in the halos, promises to produce important constraints on galactic ecology.

Acknowledgements. I thank John, Alan and Gus for organizing a very memorable meeting and a fitting tribute to OCIW's centenary. I also wish to thank Steve Allen, Meghan Gray, and David Sand for generously allowing me to present their latest work in the oral version of this review, and Harald Ebeling, Richard Ellis, Jean-Paul Kneib, Priya Natarajan, and Graham Smith for allowing me to present results from our research programs. I acknowledge support through a Royal Society University Research Fellowship and a Philip Leverhulme Prize Fellowship.

References

Abdelsalam, H. M., Saha, P., & Williams, L. L. R. 1998, AJ, 116, 1541
Allen, S. W. 1998, MNRAS, 296, 392
Allen, S. W., Schmidt, R. W., & Fabian, A. C. 2002, MNRAS, 335, 256
Athreya, R. M., Mellier, Y., van Waebeke, L., Pelló, R., Fort, B., & Dantel-Fort, M. 2002, A&A, 384, 743
Bézecourt, J., Kneib, J.-P., Soucail, G., Ebbels, T. M. D. 1999, A&A, 347, 21
Blandford, R. D., & Narayan, R. 1992, ARA&A, 30, 311
Brainerd, T. G., Blandford, R. D., & Smail, I. 1996, ApJ, 466, 623
Brainerd, T. G., Wright, C. O., Goldberg, D. M., & Villumsen, J. V. 1998, ApJ, 502, 505
Campusano, L. E., Pelló, R., Kneib, J.-P., Le Borgne, J.-F., Fort, B., Ellis, R. S., Mellier, Y., & Smail, I. 2001, A&A, 378, 394
Clowe, D., & Schneider, P. 2001, A&A, 379, 384
——. 2002, A&A, 395, 385
Cowie, L. L., Barger, A. J., & Kneib, J.-P. 2002, ApJ, 123, 2197
Dahle, H., Kaiser, N., Irgens, R. J., Lilje, P. B., & Maddox, S. J. 2002, ApJS, 139, 313
Dye, S., et al. 2002, A&A, 386, 12
Ebbels, T. M. D., Le Borgne, J.-F., Pelló, R., Ellis, R. S., Kneib, J.-P., Smail, I., & Sanahuja, B. 1996, MNRAS, 281, L75
Ebeling, H., Voges, W., Böhringer, H., Edge, A. C., Huchra, J. P., & Briel, U. G. 1996, MNRAS, 281, 799
Ellis, R. S., Santos, M. R., Kneib, J.-P., & Kuijken, K. 2001, ApJ, 560, L119
Ettori. S., & Lombardi, M. 2003, A&A, 398, L5
Fischer, P., & Tyson, A. J. 1997, AJ, 114, 14
Fort, B., Le Fèvre, O., Hammer F., & Cailloux, M. 1992, ApJ, 399, L125
Gavazzi, R., Fort, B., Mellier, Y., Pelló, R., & Dantel-Fort, M. 2003, A&A, 403, 11
Ghigna, S., Moore, B., Governato, F., Lake, G., Quinn, T., & Stadel, J. 2000, ApJ, 544, 616
Gioia, I. M., Shaya, E. J., Le Fèvre, O., Falco, E. E., Luppino, G. A., & Hammer, F. 1998, ApJ, 497, 573
Gray, M. E., et al. 2004, in preparation

Gray, M. E., Taylor, A. N., Meisenheimer, K., Dye, S., Wolf, C., & Thommes, E. 2002, ApJ, 568, 141
Hammer, F., Rigaut, F., Le Fèvre, O., Jones, J., & Soucail, G. 1989, A&A, 208, L7
Hu, E. M., Cowie, L. L., McMahon, R. G., Capak, P., Iwamuro, F., Kneib, J.-P., Maihara, T., & Motohara, K. 2002, ApJ, 568, L75
Kaiser, N., & Squires, G. 1993, ApJ, 404, 441
Kaiser, N., Squires, G., & Broadhurst, T. 1995, ApJ, 484, 460
Kneib, J.-P., Ellis, R. S., Smail, I., Couch, W. J., & Sharples, R. M. 1996, ApJ, 471, 643
Kneib, J.-P., Hudelot, P., Ellis, R. S., Treu, T., Smith, G. P., Marshall, P., Czoske, O., Smail, I., & Natarajan, P. 2004, ApJ, submitted
Kneib, J.-P., Mellier, Y., Fort, B., & Mathez, G. 1993, A&A, 273, 367
Kochanek, C. S. 1990, MNRAS, 247, 135
Lynds, R., & Petrosian, V. 1989, ApJ, 336, 1
Margoniner, V. E. 2004, in Carnegie Observatories Astrophysics Series, Vol. 3: Clusters of Galaxies: Probes of Cosmological Structure and Galaxy Evolution, ed. J. S. Mulchaey, A. Dressler, & A. Oemler (Pasadena: Carnegie Observatories, http://www.ociw.edu/ociw/symposia/series/symposium3/proceedings.html)
Margoniner, V. E., et al. 2004, in Carnegie Observatories Astrophysics Series, Vol. 3: Clusters of Galaxies: Probes of Cosmological Structure and Galaxy Evolution, ed. J. S. Mulchaey, A. Dressler, & A. Oemler (Pasadena: Carnegie Observatories, http://www.ociw.edu/ociw/symposia/series/symposium3/proceedings.html)
Marshall, P. J., Hobson, M. P., Gull, S. F., & Bridle, S. L. 2002, MNRAS, 335, 1037
Mellier, Y., Fort, B., & Kneib J.-P. 1993, ApJ, 407, 33
Miralda-Escudé, J., & Babul, A., 1995, 449, 18
Natarajan, P., Kneib, J.-P., & Smail, I. 2002, ApJ, 580, L11
Natarajan, P., Kneib, J.-P., Smail, I., & Ellis, R. S. 1998, ApJ, 499, 600
Navarro, J. F., Frenk, C. S., & White, S. D. M. 1997, ApJ, 490, 493
Ota, N., Hattori, M., Pointecouteau, E., & Mitsuda, K., 2004, A&A, submitted
Ota, N., Mitsuda, K., & Fukazawa, Y. 1998, ApJ, 495, 1700
Pettini, M., Rix, S. A., Steidel, C. C., Adelberger, K. L., Hunt, M. P., & Shapley, A. E. 2002, ApJ, 569, 742
Refregier, A., & Bacon, D. 2003, MNRAS, 338, 48
Sahu, K. C., et al. 1998, ApJ, 492, L125
Sand, D. J., Treu, T., Smith, G. P., & Ellis, R. S. 2004, ApJ, submitted
Sand, D. J., Treu, T., & Ellis, R. S. 2002, ApJ, 574, L129
Schindler, S., Hattori, M., Neumann, D. M., & Böhringer, H. 1997, A&A, 317, 646
Seitz, S., Schneider, P., & Bartelmann, M. 1998, A&A, 337, 325
Smail, I., Couch, W. J., Ellis, R. S., & Sharples, R. M. 1995, ApJ, 440, 501
Smail, I., Dressler, A. Kneib, J.-P., Ellis, R. S., Couch, W. J., Sharples, R. M., & Oemler, A., Jr. 1996, ApJ, 469, 508
Smail, I., Ivison, R. J., Blain, A. W., & Kneib, J.-P. 2002, MNRAS, 331, 495
Smith, G. P., et al. 2002, MNRAS, 330, 1
Smith, G. P., Kneib, J.-P., Ebeling, H., Czoske, O., & Smail, I. 2001, ApJ, 552, 493
Smith, G. P., Kneib, J.-P., Smail, I., Ebeling, H., Mazzotta, P., & Czoske, O. 2004, ApJ, in preparation
Soucail, G., Mellier, Y., Fort, B., Mathez, G., & Cailloux, M. 1988, A&A, 191, L19
Soucail, G., Ota, N., Böhringer, G., Czoske, O., Hattori, M., & Mellier, Y. 2000, A&A, 355, 433
Swinbank, A. M., et al. 2004, ApJ, submitted
Tyson, J. A., Kochanski, G. P., & dell'Antonio, I. P. 1998, ApJ, 498, L107
Tyson, J. A., Wenk, R. A., & Valdes, F. 1990, ApJ, 349, L1
van der Werf, P., Knudsen, K. K., Kneib, J.-P., & Smail, I. 2004, in preparation
Wambsganss, J., Giraud, E., Schneider, P., & Weiss, A. 1989, ApJ, 337, L73
Wehner, E. H., Barger, A. J., & Kneib, J.-P. 2002, ApJ, 577, L83
Williams, L. L. R., Navarro, J. F., & Bartelmann, M. 1999, ApJ, 527, 535
Worrall, D. M., & Birkinshaw, M. 2003, MNRAS, 340, 1261
Wu, Z.-P., & Fang, L.-Z. 1997, ApJ, 483, 62
Xue, S.-J., & Wu, X.-P. 2002, ApJ, 576, 152